High-Performance Nanocatalysts for Single-Step Hydrogenations

JOHN MEURIG THOMAS,*,†,‡
BRIAN F. G. JOHNSON,*,§ ROBERT RAJA,*,†,§
GOPINATHAN SANKAR,† AND
PAUL A. MIDGLEY‡

Davy Faraday Research Laboratory, The Royal Institution of Great Britain, 21 Albemarle Street, London W1S 4BS, U.K., Department of Materials Science, University of Cambridge, Cambridge CB2 3QZ, U.K., and University Chemical Laboratory, Lensfield Road, Cambridge CB2 1EW, U.K.

ABSTRACT

Bimetallic nanoparticles (Ru_6Pd_6, Ru_6Sn, $Ru_{10}Pt_2$, Ru_5Pt, $Ru_{12}Cu_4$, and $Ru_{12}Ag_4$) anchored within silica nanopores exhibit high activities and frequently high selectivities, depending upon the composition of the nanocatalyst, in a number of single-step (and often solvent-free) hydrogenations at low temperatures (333–373 K). The selective hydrogenations of polyenes (such as 1,5,9-cyclododecatriene and 2,5-norbornadiene) are especially efficient. Good performance is found with these nanoparticle catalysts in the hydrogenation of dimethyl terephthalate to 1,4 cyclohexanedimethanol and of benzoic acid to cyclohexanecarboxylic acid or to cyclohexene-1-carboxylic acid, and also in the conversion of benzene to cyclohexene (or cyclohexane), the latter being an increasingly important reaction in the context of the production of Nylon. Isolated atoms of noble metals (Pd, Rh, and Pt) in low oxidation states, appropriately complexed and tethered to the inner walls of nanoporous (ca. 3 nm diameter) silica, are very promising enantioselective hydrogenation catalysts. Nanoporous carbons, as well as other nanoporous oxides, may also be used to anchor and tether the kind of catalysts described here.

I. Introduction

This Account is primarily concerned with supported, bimetallic catalysts that are so small (1–1.5 nm diameter) that essentially all the atoms in the nanoparticles are exposed to reactant species. Moreover, the individual nanoparticles are distributed and anchored in a spatially uniform manner along the inner walls of high-area (500–900 m² g⁻¹) nanoporous silica supports, the sharply defined pore diameter of which is controllable within the range 3–30 nm. Because the nanocatalysts are firmly anchored to the walls of these (relatively large) pores, their tendency to sinter and coalesce (with consequential loss of active area) is minimized, and, in addition, there is essentially free diffusional access of reactants to, and egress of products from, the nanoparticle catalyst, thereby facilitating the catalytic turnover of quite bulky organic molecules.[1,2] The essential architectural features of these novel nanocatalysts are depicted in Figure 1.

This Account also deals briefly with the promising performance of enantioselective hydrogenation catalysts

* To whom correspondence should be addressed. For J.M.T.: tel. +44 207-670-2928, fax +44 207-670-2988, e-mail dawn@ri.ac.uk. For B.F.G.J.: tel. +44-1223-336337, fax +44-1223-336017, e-mail bfgj1@cam.ac.uk. For R.R.: tel. +44 1223-336335, fax +44 1223-336017, e-mail robert@ri.ac.uk.
† The Royal Institution of Great Britain.
‡ University of Cambridge.
§ University Chemical Laboratory.

Brian F. G. Johnson, Fellow of the Royal Society (FRS), the Royal Society of Edinburgh (FRSE), the Royal Society of Chemistry (FRSC), and of the Academia Europa was awarded the Corday-Morgan Medal in 1984, The Royal Society of Chemistry Prize for Transition Metal Chemistry in 1986, the Tilden Medal in 1994, and the Frankland Medal (RSC) in 2002. He has been Visiting Professor at numerous universities throughout the world and has delivered named lectures at a wide variety of institutions. In 1998, he was awarded the Grand Cross of Brazil for his contributions to science. He is among the top 25 most cited physical scientists in the UK and the top 100 worldwide. His grant income from the EPSRC (UK) places him in the top 20 from all areas of engineering and the physical sciences.

Robert Raja received his masters degree in chemistry (honors) at the Birla Institute of Technology and Science and completed his Ph.D. on inorganic solid mimics of enzyme catalysts with Paul Ratnasamy at the National Chemical Laboratory, Pune, India (1997). He was awarded The Royal Commission of 1851 Exhibition to pursue his research at the Davy Faraday Research Laboratory of the Royal Institution of Great Britain (1997–1999), where he worked on the shape-selective and regiospecific oxyfunctionalization of hydrocarbons and aromatics in air, while simultaneously broadening his interests in solid-state, surface, and materials chemistry. He is currently a Peterhouse Senior Research Associate and has a joint appointment with Bayer A.G., Leverkusen, Germany, and at the Department of Chemistry, University of Cambridge. His research interest focuses on designing novel microporous, bimetallic nanoparticles and constrained chiral catalysts for environmentally benign selective oxidation and hydrogenation processes. He is the author of over 45 research publications and is the inventor of 10 international patents.

Gopinathan Sankar took his initial degree at the University of Madras and completed his Ph.D. at the Solid State and Structural Chemistry unit, Indian Institute of Science, Bangalore, in 1986. He joined Davy Faraday Research Laboratory, The Royal Institution of GB, London, in 1990 as a postdoctoral research fellow, where he broadened his research in the area of microporous and mesoporous catalysts, in addition to his efforts in the development of in situ methods for synchrotron radiation-based techniques to characterize catalysts under operating conditions. Currently he is a senior research fellow at the Royal Institution and a Reader at the University College London.

Paul Midgley is a University Senior Lecturer and Director of the Electron Microscopy Facility at the Department of Materials Science and Metallurgy. Before moving to Cambridge in 1997, he held two research fellowships in the H.H. Wills Physics Laboratory at the University of Bristol, the first funded by The Royal Commission for The Exhibition of 1851, the second by The Royal Society. He has studied a wide variety of materials by electron microscopy and developed a number of novel electron microscopy techniques. Recently, he and his research group have developed new analytical techniques using EFTEM, STEM, and electron holography and applied these to materials systems at the nanometer level. His recent work on electron tomography has been much acclaimed. He has written over 100 articles and is invited regularly to speak at conferences around the world.

John Meurig Thomas graduated from the University of Wales, Swansea, in 1954. From 1978 to 1986, he was the Head of the Department of Physical Chemistry, University of Cambridge. From 1986 to 1991, he was the Director of the Royal Institution of Great Britain, London, and of the Davy Faraday Research Laboratory there, where he occupied the Chair created for Michael Faraday. He now works partly at the Royal Institution and partly at Cambridge. His awards for solid-state, materials, and surface chemistry include the Davy Medal, Rutherford and Bakerian Lectureships of the Royal Society, the Faraday Medal (and five others) of the Royal Society of Chemistry, the Messel Gold Medal of the Society of Chemical Industry, the Willard Gibbs Gold Medal of the American Chemical Society, and the Semenov Medal of the Russian Academy. The European Federation of Catalyst Societies elected him their first peripatetic Francois Gault lecturer, and, in 1999, he became the first recipient of the ACS award for creative research in homogeneous and heterogeneous catalysis. His Royal Institution Christmas Lectures on crystals were broadcast nationally on BBC TV in 1987 and 1988. In 1991, he was knighted for his services to chemistry and the popularization of science.
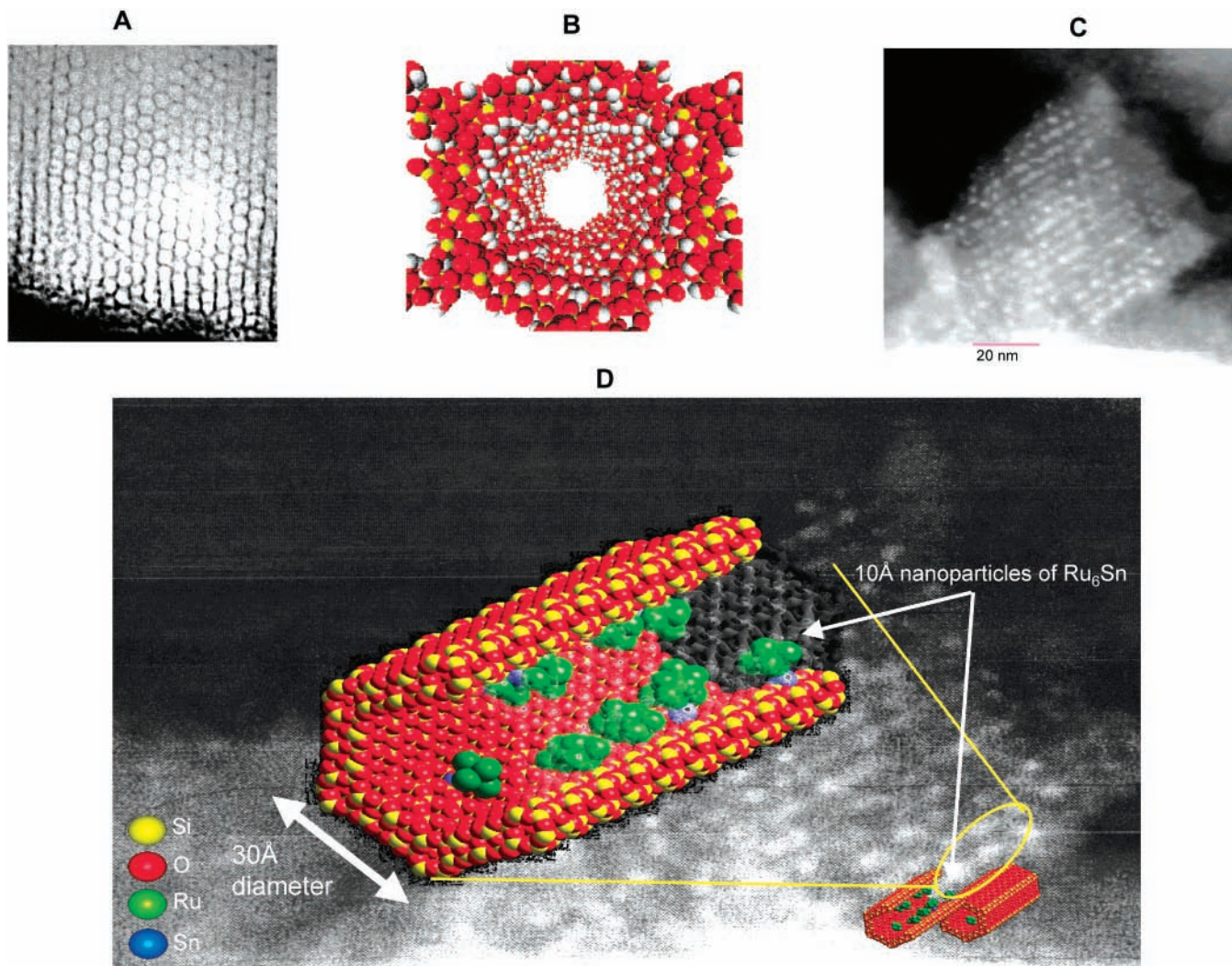
FIGURE 1. (A) High-resolution electron micrograph of a typical hexagonal array of nanopores in silica (10 nm diameter). (B) Computer graphic representation of the interior of a single pore of the silica, showing the pendant silanol groups. (C) High-angle annular dark-field (scanning electron transmission) micrograph showing the distribution of anchored Ru_6Sn nanoparticles within the nanopores of the siliceous host. (D) Computer graphic illustration of the Ru_6Sn nanoparticles superimposed on an enlargement of the electron micrograph shown in (C).

formed by tethering, inside siliceous nanopores, chirally biased, appropriately complexed, single atoms of noble metals in low oxidation states.[3] The essential features of such heterogenized homogeneous catalysts are summarized in Figure 2.

When, five years ago, we and our colleagues embarked[4] on these studies, we were motivated by several perceived advantages. First, we were already aware (from IR, NMR, and other evidence) that gentle thermolysis of metal cluster (and mixed-metal cluster) carbonylates, when attached to oxide surfaces rich in pendant hydroxyl groups, could yield individual (bare), decarbonylated metallic or bimetallic nanoparticles strewn across the oxide surfaces to which the carbonylate species had originally been attached. (We soon confirmed this fact in a series of combined in situ XAFS and IR studies; the results obtained with a typical mixed-metal parent carbonylate $[Ru_{12}C_2(CO)_{32}Cu_4Cl_2]^{2-}$ anion are shown in Figure 3.)

Second, we were also aware that, potentially, a vast number[5] of precursor metal and mixed-metal carbonyl-

ates, of well-defined structure and stoichiometry, was available for the production of a wide range of novel nanocatalysts. A small selection of such precursor materials, shown in Figure 4, illustrates the veracity of this statement. The great merit of preparing bimetallic nanocatalysts from such precursors is that it guarantees—as many subsequent elemental fingerprinting and electron microscopic imaging studies have repeatedly confirmed[6]— the integrity (and stoichiometry) of the nanoparticle catalyst, an end that is very difficult to achieve using incipient wetness and other methods of preparation.

Third, it had already been established[7] in other contexts—involving high-temperaure, hydrocarbon reforming catalysis—that there was special merit in using bimetallic, rather than monometallic, nanoparticles in that their catalytic performance is generally far superior to that of the single nanometal alone. For example, we quickly discovered[4c] that nanoparticles of Pd and Ru alone were each far less active and less selective as hydrogenation catalysts than their Pd_6Ru_6 nanoparticle counterparts. We also noted that bimetallic nanocatalysts were more resis-
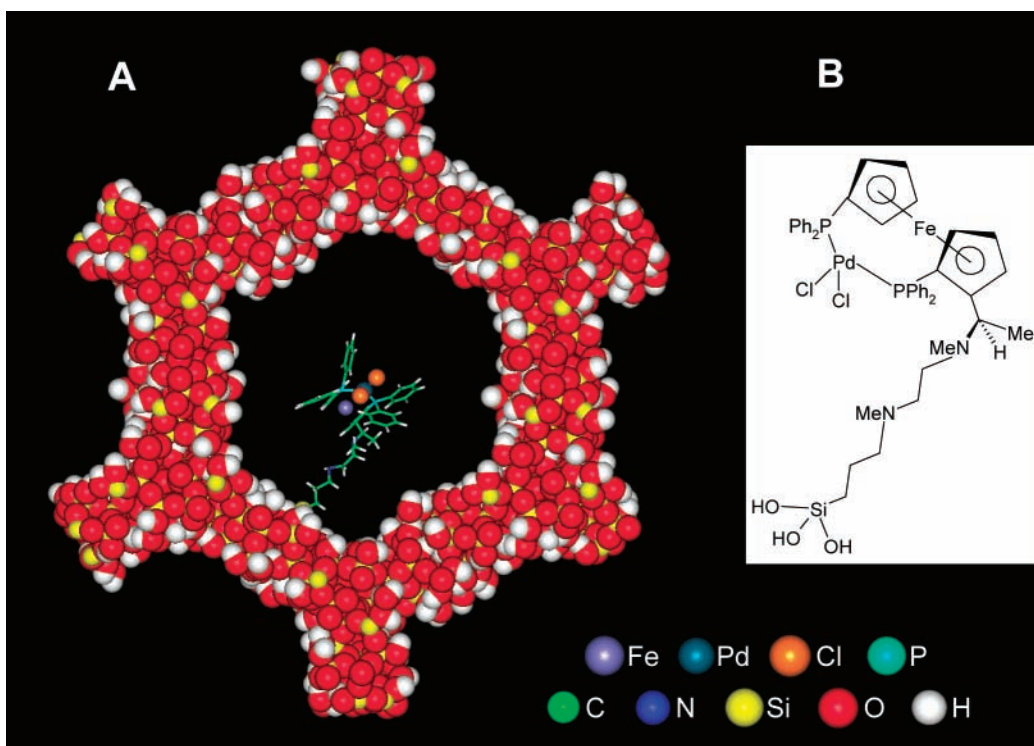
FIGURE 2. Schematic drawing illustrating the nature of a tethered Pd (diphenylphosphino-ferrocenyl-diamine) complex, chirally constrained within a siliceous nanopore.

tant to sulfur poisoning (in their role as facilitators of naphthalene partial hydrogenation) than the separate components alone (as nanocatalysts).

Fourth, special preparative in situ X-ray absorption spectroscopic (and other) techniques,[8] allied with powerful ex situ high-resolution electron microscopic ones,[6] were available for the determination of the detailed atomic structure of the bare, supported bimetallic nanoparticles. Moreover, we were fully aware of the encouraging prospect of being able to define the precise spatial location and topography of supported nanoparticles through the technique of electron tomography (and allied procedures, such as Rutherford backscattered electron imaging) that were then under development (see Figure 5) and which have subsequently come to fruition.[9]

Last, and not least, with the impending arrival of the so-called hydrogen economy[10] and the parallel, universal drive toward clean technology, there was a pressing need for the discovery and development of single-step (and preferably solvent-free) highly active and highly selective catalysts for the hydrogenation of a growing range of key organic compounds.[11] In the future, with the decline of chemical feedstocks from fossil fuels, and the concomitant growth of those extracted from readily sustainable plant sources, the fraction of organic molecular products that are manufactured industrially by direct hydrogenation is inevitably destined to rise.[12] A particularly interesting example, symptomatic, we believe, of possible future developments, is contained in the work of Draths and Frost.[12] These workers addressed the problems of petroleum-based feedstocks, toxic starting materials or reagents, and generation of environmentally incompatible

byproducts, and they proceeded to evolve a biosynthetic pathway that microbially converted D-glucose into *cis,cis*-muconate, which is then hydrogenated (using a platinum-on-carbon catalyst) to yield the adipate:

$$ ^-O_2C \diagup\!\!\!\diagdown\!\!\!\diagup\!\!\!\diagdown CO_2^- \xrightarrow[\text{Pt/C}]{H_2} \,^-O_2C \diagup\!\!\!\diagdown\!\!\!\diagup CO_2^- $$
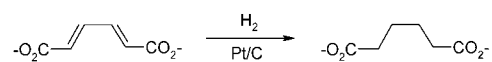
Efficient, high-performance new catalysts, operating under mild and environmentally benign conditions, are therefore an exigent need. Here we describe several of them.

We are conscious of the fact the physicochemical tools that we have so far harnessed for our studies, though quite sophisticated, are not by any means complete. Thus, we have determined the atomic structure of our nanocatalysts under atmospheric pressure, whereas, ideally, what is required—as with our other studies[3c,8]—are structural studies under operating pressures of 10−30 bar. Moreover, although the theoretical tools (such as density functional theory) that we have used are very illuminating,[8b,13] it will be necessary soon to address questions relating to the electronic states of the orbitals associated with active nanoparticle catalysts. Such plans are in hand. But our experimental results to date, which encompass a variety of hydrogenations, have their own validity. One particular merit that our method of producing and anchoring the nanoparticle catalysts possesses is that, unlike colloidal metals (studied catalytically by pioneers such as Rideal and Turkevich[14]), where the colloidal metals are susceptible to coalescence and sintering and which therefore deactivate rapidly, our nanocatalysts retain their high performance for prolonged periods.
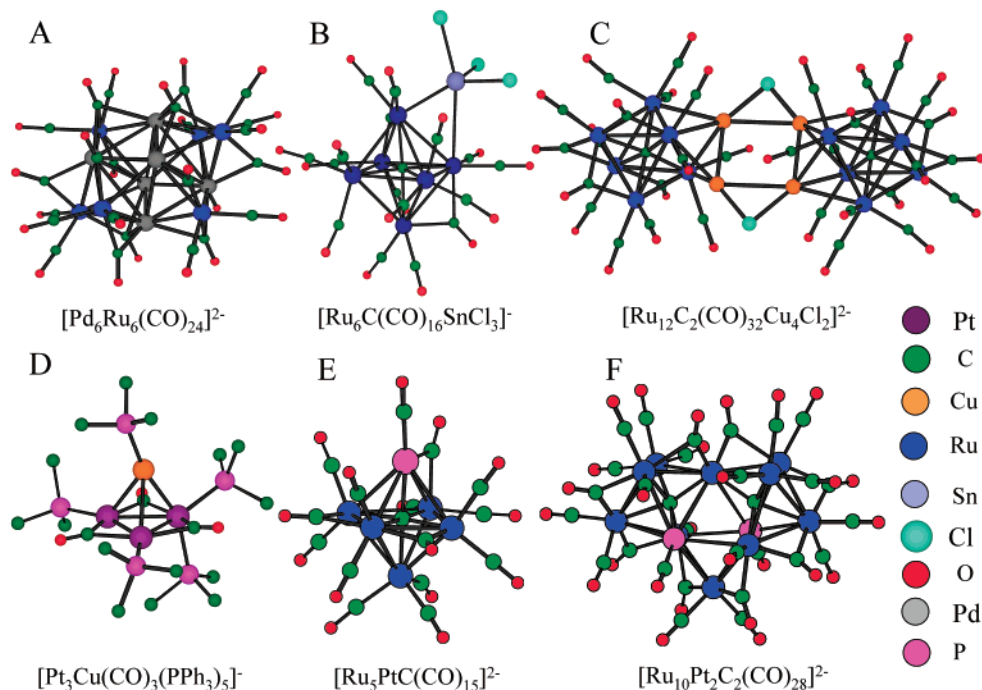
FIGURE 3. Fourier transform of (a) the Ru K-edge and (b) the Cu K-edge EXAFS data recorded during the thermolysis of the $Ru_{12}Cu_4C_2$ catalyst anchored on silica. (c) The model derived[13] from a force field, energy minimization calculation using ESFF interatomic potentials. (d) DFT-optimized structure of the silica-bound $Ru_{12}Cu_4C_2$ cluster. The distances (in angstroms) include all independent bonds. (e) Comparison of the Cu K-edge EXAFS data with the spectrum calculated taking the structural details obtained from the DFT calculation using this structure.[8b]

II. Preparation and Structural Characterization of the Nanocatalysts

As described previously,[4] salts of the respective mixed-metal carbonylate (typically $[Pd_6Ru_6(CO)_{24}]^{2-}2[N(C_2H_5)_4]^+$) were loaded into mesoporous silica supports (typically MCM-41 with sharply defined pore diameter of 3 nm; or STAC-1,[15] pore diameter 5−8 nm; or SBA-15,[15] pore diameter 3−30 nm) by making a slurry in diethyl ether/dichloromethane. The silica-encapsulated clusters, such as $[Ru_6C(CO)_{16}Cu_2Cl]^{2-}(PPN)_2$ (where PPN = bis(triphenylphosphane)iminium), were activated by heating to ca. 195 °C in vacuo for 2 h or so. Earlier in situ FTIR spectroscopic studies showed that no residual peaks corresponding to the carbonyl frequencies remained after this treatment, and the chlorine is carried away as phosgene during the thermolysis.

Near-edge (XANES) and extended-edge (EXFAS) data were collected at Station 9.2 of the Daresbury Synchrotron Laboratory. This operates at 2 GeV, and a typical currents fall in the range 150−250 mA. Full details of the data processing and related procedures have been described elsewhere.[8,16] Gates and others[17] have also shown how EXAFS data may be used to determine the structures of decarbonylated monometallic {e.g., $Ir_4(CO)_{12}$ or $Rh_6(CO)_{16}$}

and bimetallic {e.g., $Re_2Pt(CO)_{12}$} clusters laid down on high-area supports. They point out that when such clusters are decarbonylated within the cages of zeolites (like the faujasitic cage in Na-X), the bare cluster essentially retains the skeletal structure of the parent carbonylate, as is the case for Ir_4 derived from its dodeca-carbonyl analogue, but that when supported on γ-alumina a new structure is adopted by the six-atom (Re_4Pt_2) cluster.

It is worth emphasizing that new insights into the atomic structure of supported bimetallic nanocatalysts are derived from a combination of molecular mechanics and ab initio techniques.[13] The best local structural information is obtained initially from XAFS (i.e., XANES and EXAFS). Such data are, however, one-dimensional in nature, as only average information on interatomic distances and coordination can be derived. XAFS alone cannot solve the structure of the cluster: augmentation by computation is essential. Our XAFS results clearly show that, in the Ru−Cu[4b] and Ru−Sn[1] bimetallic nanocatalysts described herein, the nanoclusters are anchored to the mesoporous silica via oxygen (the same is true for the Ru−Ag[4a] cluster described previously). By a sophisticated procedure of simultaneous refinement of the EXAFS data of (for example) both the Ru and Cu K-edges, we could

FIGURE 4. Typical parent anionic carbonylates from which naked nanoparticle (10—15 Å diameter, depending upon the constituents of the bimetallic core) catalysts are generated. (A) $[Pd_6Ru_6(CO)_{24}]^{2-}$, (B) $[Ru_6C(CO)_{16}SnCl_3]^-$, (C) $[Ru_{12}C_2(CO)_{32}Cu_4Cl_2]^{2-}$, (D) $[Pt_3Cu(CO)_3(PPh_3)_5]^-$, (E) $[Ru_5PtC(CO)_{15}]^{2-}$, and (F) $[Ru_{10}Pt_2C_2(CO)_{28}]^{2-}$.

unambiguously establish the nature of the anchoring of the decarbonylated cluster to the silica.

The catalytic testing was carried out in a high-pressure stainless steel reactor (Cambridge Reactor Design) lined with poly ether ether ketone (PEEK).[1,2] Nanoparticle bimetallic catalyst (typically 20 mg) was activated (463 K for 2 h in the presence of H_2 {0.5 MPa}) prior to studying the hydrogenation reaction. The reactor was then depressurized and cooled to room temperature before introduction of the substrate (reactant), typically some 50 g, and an internal standard such as mesitylene (2.5 g). The vessel was pressurized with H_2 (30 bar) and heated to the desired temperature with continued stirring (400 rpm). During the reaction, small aliquots were removed using a mini-robot autosampler to enable the kinetics to be followed. (It was sometimes necessary to use a benign solvent when the reactants were solid at room temperature—as is the case with dimethyl terephthalate, DMT;[2] see Table 1.) Reaction products and unconverted reactants were analyzed with gas chromatography, and the identity of the products was confirmed by LC—MS (Shimadzu QP 8000).

Electron microscopy was carried out mainly using a VG HB501 field-emission scanning transmission instrument (both low- and high-angle annular dark-field (HAADF) detector) as previously described.[6] It was also possible to record HAADF electron tomography as previously described.[9] A typical result of dark-field (Rutherford scattering) electron tomographic analysis of the supported bimetallic nanocatalysts is shown in Figure 5.

So far as preparing the chirally biased, single-atom catalysts anchored on the inner walls of the silica nanopores is concerned, the procedure is outlined in Figure 6.
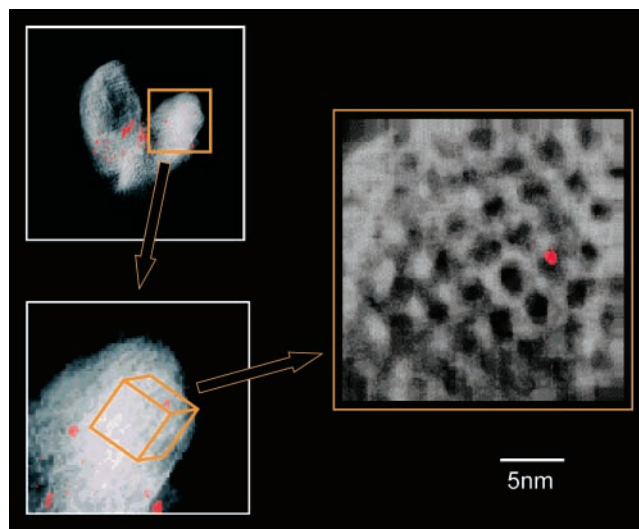

FIGURE 5. Illustration of how an individual nanoparticle catalyst of Pd_6Ru_6, diameter ca. 1 nm (color coded), may be isolated in the digitally reconstructed tomographic data (see ref 9 and http://www-hrem.msm.cam.ac.uk/~mw259/Work/Tomo.html for further details) so as to show that it is embedded within, and anchored to, the wall of, nanoporous silica. The scale bar corresponds to images recorded at the highest magnification.

Here, care is taken to ensure that active sites are grafted only to the inner walls of the silica by first deactivating the external surface using dichlorodiphenylsilane (Ph_2-$SiCl_2$) under nondiffusive conditions.[3b] The full derivatization of the inner walls, as previously described, is achieved with reagents such as 3-bromopropyltrichlorosilane. Solid-state, multinuclear (MAS) NMR as well as FTIR and, where appropriate, XAFS analysis were used to characterize these catalysts.[3]
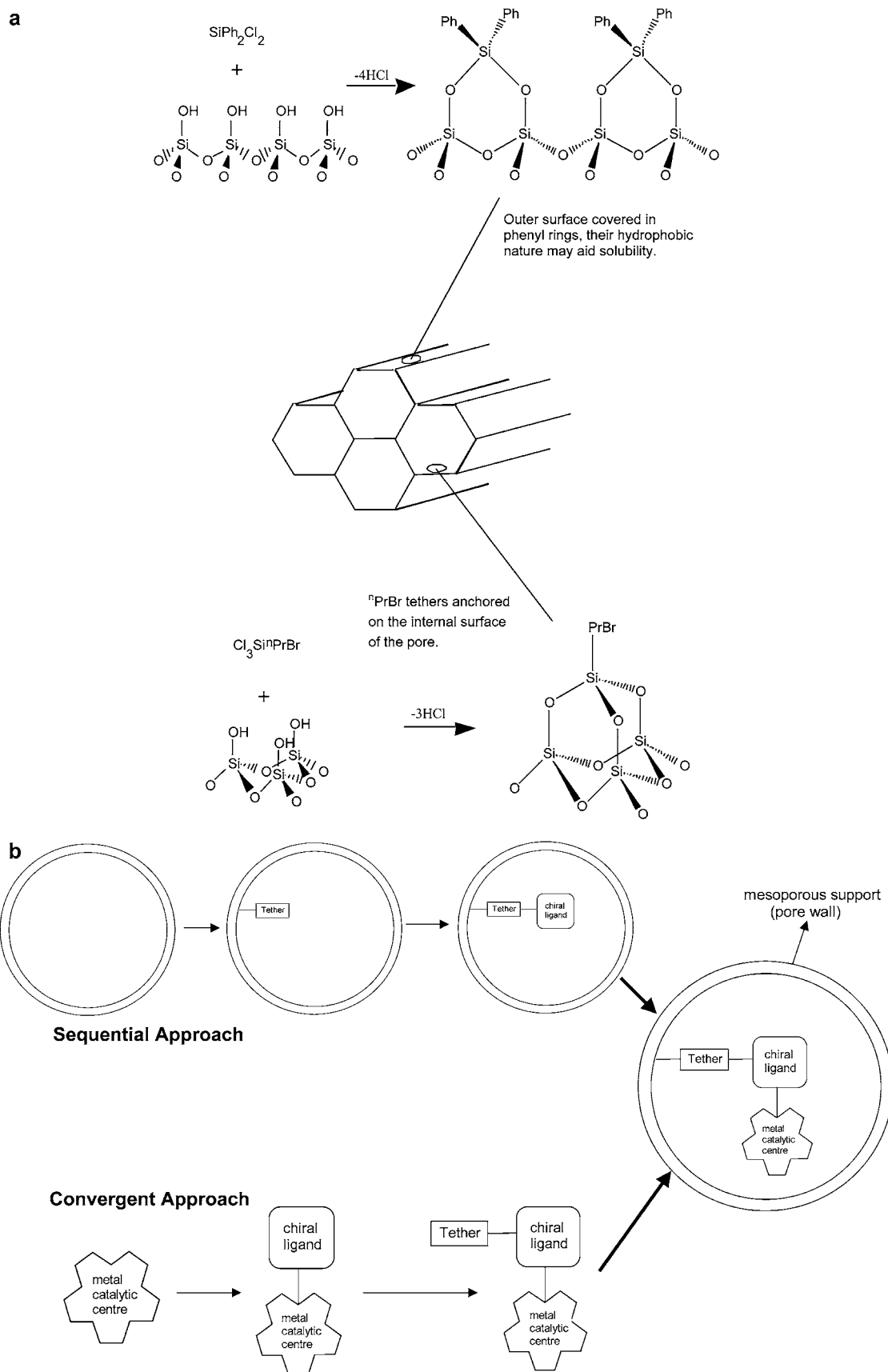
FIGURE 6. (a) Sequence of steps outlining the synthesis of the activated MCM-41. The mesoporous framework was first treated with Ph_2SiCl_2 under nondiffusive conditions to deactivate the exterior walls of the material, followed by the derivatization of the interior walls with 3-bromopropyltrichlorosilane to yield the activated MCM-41. (b) Schematic of the two approaches used to anchor the chiral catalyst onto the mesoporous silica surface.

Table 1. Single-Step Hydrogenations of Cyclic Polyenes and Aromatics—Comparison of Catalysts (See Figure 7 for Description of Products)[a]

Catalyst encapsulated in mesoporous SiO₂	Substrate	Solvent	Time (h)	Temp (K)	Conv (mol %)	TOF (h⁻¹)	Product distribution (mol %)			
							A	B	C	D
Pd₆Ru₆	1,5-cyclooctadiene	-	8	353	36.9	2012	15.7	84.5	-	-
Ru₆Sn	1,5-cyclooctadiene	-	8	353	11.7	1980	100	-	-	-
Cu₄Ru₁₂	1,5-cyclooctadiene	-	8	353	11.5	690	70.4	29.2	-	-
Ag₄Ru₁₂	1,5-cyclooctadiene	-	8	353	9.0	465	57.3	42.5	-	-
Pd₆Ru₆	1,5,9-cyclododecatriene	-	8	373	64.9	5350	-	11.7	88.5	-
Ru₆Sn	1,5,9-cyclododecatriene	-	8	373	17.2	1940	17.2	82.4	-	-
Pd₆Ru₆	2,5-norbornadiene	-	8	333	76.4	11176	24.7	75.1	-	-
Ru₆Sn	2,5-norbornadiene	-	8	333	51.4	10210	88.6	11.3	-	-
Ru₅Pt₁	benzene	-	6	353	36.2	2625	8.7	91.2	-	-
Ru₁₀Pt₂	benzene	-	6	353	27.6	1790	24.9	75.2	-	-
Pd₆Ru₆	benzene	-	6	353	58.7	3216	-	100	-	-
Ru₆Sn	benzene	-	6	353	17.5	953	11.7	88.1	-	-
Cu₄Ru₁₂	benzene	-	6	353	11.7	480	-	100	-	-
Ru₅Pt₁	Dimethyl terephthalate	C₂H₅OH	4	373	7.5	155	58.7	33.5	-	6.9
Ru₁₀Pt₂	Dimethyl terephthalate	C₂H₅OH	4	373	23.3	714	42.6	52.3	-	-
Pd₆Ru₆	Dimethyl terephthalate	C₂H₅OH	8	373	15.5	125	22.5	4.2	-	74.2
Ru₆Sn	Dimethyl terephthalate	C₂H₅OH	8	373	5.3	54	77.2	-	22.6	-
Cu₄Ru₁₂	Dimethyl terephthalate	C₂H₅OH	24	373	14.2	45	25.3	63.2	-	11.3
Ru₅Pt₁	benzoic acid	C₂H₅OH	24	373	61.2	167	86.5	13.3	-	-
Ru₁₀Pt₂	benzoic acid	C₂H₅OH	24	373	78.5	317	99.5	-	-	-
Pd₆Ru₆	benzoic acid	C₂H₅OH	24	373	44.5	126	61.5	39.2	-	-
Ru₆Sn	benzoic acid	C₂H₅OH	24	373	15.9	24	9.0	42.5	48.3	-
Cu₄Ru₁₂	benzoic acid	C₂H₅OH	24	373	21.8	48	-	79.6	21.2	-

[a] Reaction conditions: catalyst, 20 mg; H₂ pressure, 20 bar; TOF = [(mol$_{substr}$)(mol$_{cluster}$)$^{-1}$ h^{-1}]. Note: Mesoporous SiO₂ used here is of the MCM-41 type.
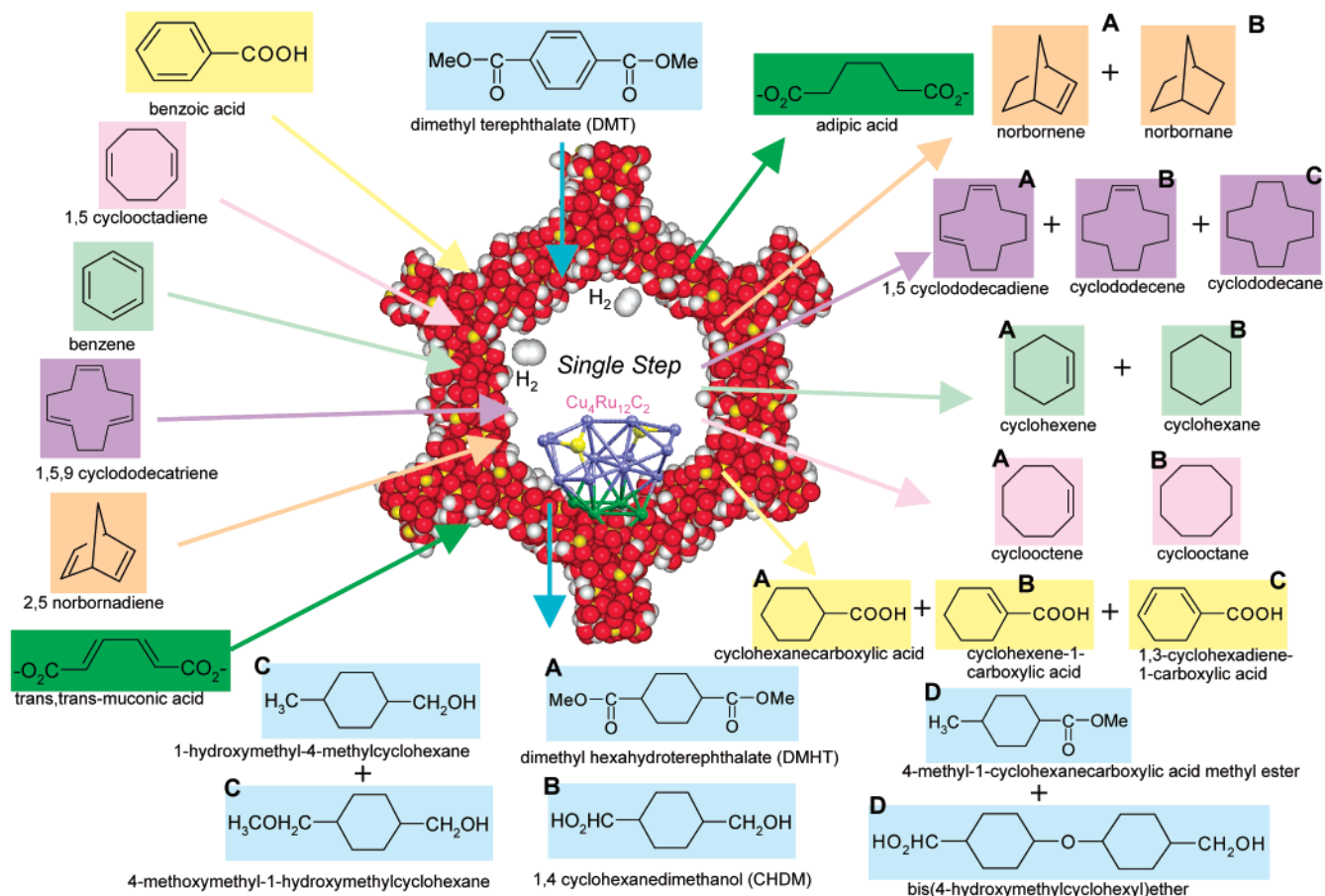

FIGURE 7. Single-step hydrogenation of some key organic compounds using highly active and selective anchored, bimetallic nanoparticle catalysts (Cu₄Ru₁₂C₂, in this case). Note: A, B, C, and D correspond to the products as listed in Table 1 (under "product distribution").

III. Specific Examples

Table 1 and Figure 7 summarize the hydrogenation results obtained with a variety of the bimetallic nanocatalysts studied by us. The results fall into two main categories, which we now discuss separately: those that operate under solvent-free conditions and those that require a (benign) solvent.

a. Low-Temperature, Solvent-Free Selective Hydrogenations of Polyenes Using Bimetallic Nanocatalysts. An instructive example of molecularly selective bimetallic nanocatalysts is seen in the solvent-free conversion of polyenes by Ru_6Sn and some other Ru-containing bimetallic analogues. The polyenes in question are 1,5,9-cyclododecatriene, 1,5-cyclooctadiene, and 2,5-norbornadiene.[1] The monoenes of all these polyenes are used extensively as intermediates in the synthesis of bicarboxylic aliphatic acids, ketones, cyclic alcohols, and lactones and for other purposes. Moreover, the selective hydrogenation of 1,5,9-cyclododecatriene to cyclododecene and cyclododecane is industrially important in the synthesis of valuable organic and polymeric intermediates, such as 12-laurolactam and dodecanedioic acid, which are important monomers for synthesis of Nylon 12, Nylon 612, copolyamides, and polyesters and for applications in coatings.

A wide variety of homogeneous and heterogeneous hydrogenation catalysts such as Raney nickel, palladium, platinum, cobalt, and mixed-transition-metal complexes have been previously used for the above-mentioned hydrogenations. But all these reactions entailed the use of organic solvents (such as *n*-heptane and benzonitrile), and some required utilization of hydrogen donors (such as 9,10-dihydroanthracene)—often at temperatures in excess of 300 °C—to achieve the desired selectivities.

Anchored Ru_6Sn nanocatalysts, such as that depicted in Figure 1D, as well as three other bimetallic nanocatalysts (see Table 1 and Figure 8), are very active—note the high turnover frequencies (TOFs) enumerated in Table 1—for the solvent-free hydrogenation of 1,5,9-cyclododecatriene. Importantly, the selectivities may be fine-tuned by adjusting the temperature (Figure 8b) and, to some degree, the contact times (Table 1). The solvent-free hydrogenation of 1,5-cyclooctadiene is also efficiently catalyzed by Ru_6Sn as well as by other Ru-containing nanocatalysts. For the hydrogenation of 2,5-norbornadiene, the TOFs for both Ru_6Sn and Ru_6Pd_6 are exceptionally large, but in the former (at 333 K) the ratio of norbornene to norbornane is 8:1, whereas for the latter it is 1:3.

Preliminary experiments also show that low-temperature, solvent-free selective hydrogenation of benzene[18a−c] to cyclohexene (an important intermediate in a new industrial method for producing adipic acid via cyclohexanol[18d]) may be effected with some of our bimetallic nanocatalysts.

b. Low-Temperature, Single-Step Hydrogenations of Some Key Organic Compounds. Here we describe the promising performance of two, related new bimetallic nanocatalysts, $Ru_{10}Pt_2$ and Ru_5Pt, for the hydrogenation
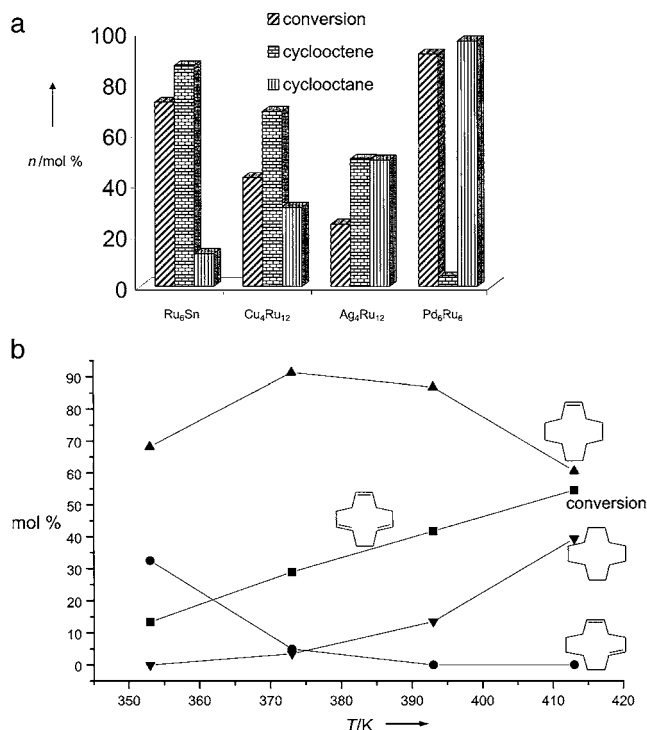

FIGURE 8. (a) Comparison of the catalytic performance and degree of selectivity for the single-step, solvent-free hydrogenation of 1,5-cyclooctadiene, using various anchored, bimetallic nanoparticle catalysts. Reaction conditions: substrate, ∼50 g; catalyst, 25 mg; H_2 pressure, 30 bar; temperature, 353 K; time, 24 h. (b) The effect of temperature on the activity and selectivity in the solvent-free hydrogenation of 1,5,9-cyclododecatriene using the anchored Ru_6Sn catalyst.

Scheme 1. Two-Step Hydrogenation of Dimethyl Terephthalate (DMT) to 1,4-Cyclohexanedimethanol (CHDM)
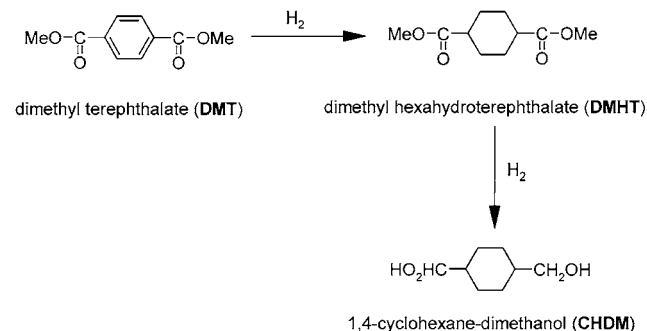
of (i) dimethyl terephthalate (DMT) to 1,4-cyclohexanedimethanol (CHDM) and (ii) benzoic acid to cyclohexanecarboxylic acid.[2]

It is noteworthy that CHDM is now preferred over ethylene glycol as a stepping stone in the production of polyester fibers (for extensive use in photography and in other applications involving polycarbonates and polyurethanes). It is also relevant to note that, to date, the only reported feasible catalytic route to CHDM is a two-step process, via dimethyl hexahydroterephthalate (DMHT), using a rhodium complex tethered on silica-supported palladium using Angelici's special catalyst[19] (Scheme 1).

Since DMT is a solid at the low temperatures at which our catalytic hydrogenations are conducted, an environ-
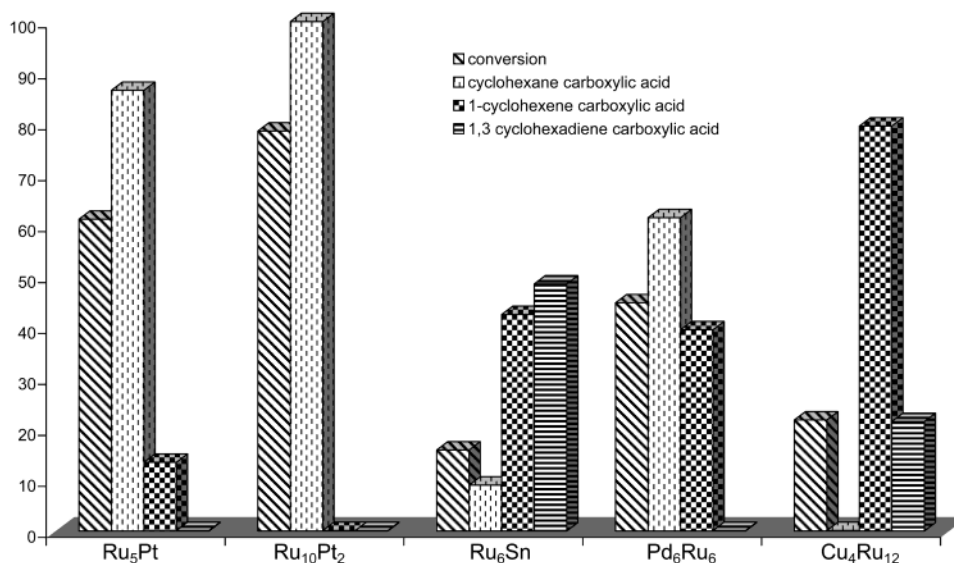
FIGURE 9. Bar chart summarizing the relative performances and selectivities of the Ru_5Pt and $Ru_{10}Pt_2$ catalysts when compared to other bimetallic nanocatalysts (used by us in our previous studies[1,4b,c]) for the hydrogenation of benzoic acid. Note that the Ru_5Pt and $Ru_{10}Pt_2$ catalysts display a high degree of selectivity for the cyclohexanecarboxylic acid, in marked contrast to the other bimetallic analogues. Reaction conditions: benzoic acid, ~2.5 g (dissolved in 75 mL of ethanol); catalyst, 50 mg; H_2 pressure, 20 bar; temperature, 373 K; time, 24 h.
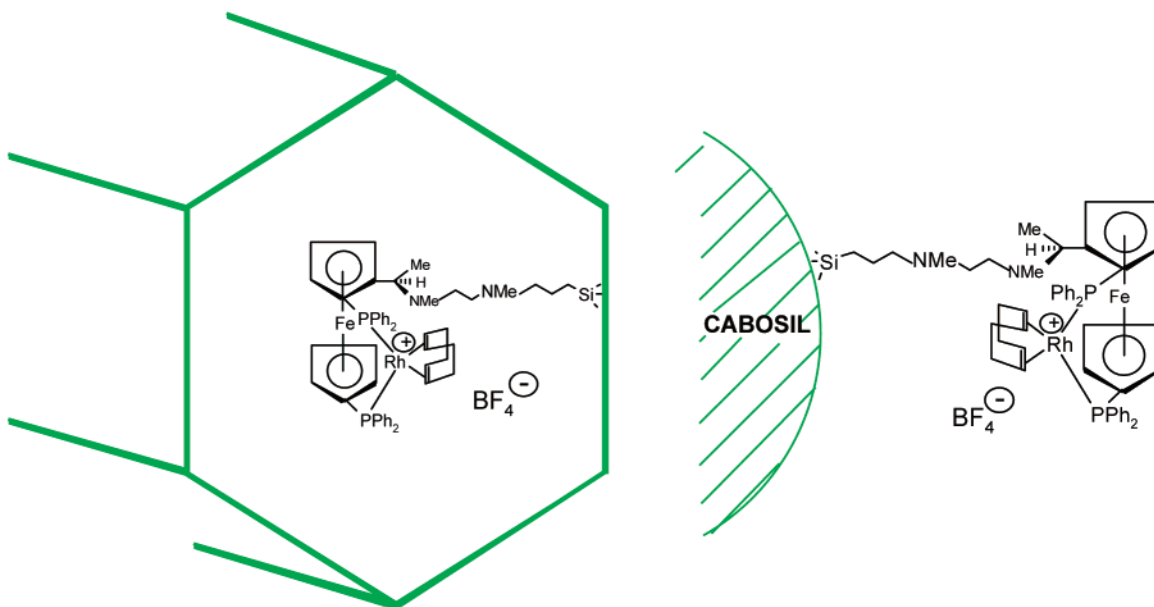
FIGURE 10. Depiction of the catalytically active dppf-ferrocenyl-Rh-COD catalyst, bound in a constrained manner to the inner walls of mesoporous silica (left) and attached to a nonporous silica (right).

mentally benign solvent (ethanol) was used to facilitate liquid–solid catalysis. Table 1 shows that more CHDM is produced than DMHT (the only other product) when $Ru_{10}Pt_2$ nanocatalysts are used. With $Ru_{12}Cu_4$, tested for comparison, there is an even higher ratio of CHDM to DMHT than with $Ru_{10}Pt_2$, but at substantially lower conversion and turnover frequency (Table 1).

The industrial interest in cyclohexanecarboxylic acid stems from the fact that, upon treatment with $NOHSO_4$ (in the presence of strong acids), it yields caprolactam, a stepping stone in one of the routes in the manufacture of Nylon.[20] Again, our new bimetallic nanocatalyst, $Ru_{10}Pt_2$, is exceptionally efficient both in selectivity (99+% toward the desired product) and in extent of conversion and TOF

(activity) compared with other analogous nanocatalysts studied by us (see Figure 9).

c. One-Step, Enantioselective Reductions Using a Tethered, Complexed, Noble-Metal Catalyst. By extending a principle first conceived[21] seven years ago (and summarized pictorially in Figures 2 and 6), whereby a designed active center attached to a chiral ligand is tethered at the inner walls of mesoporous silica (pore diameter ca. 3 nm), it is possible to produce an efficient enantioselective catalyst for the direct hydrogenation of a number of unsaturated organic molecules that are of considerable commercial importance.[22]

The conceptual methodology entails identifying a proven homogeneous catalyst and tethering it within the
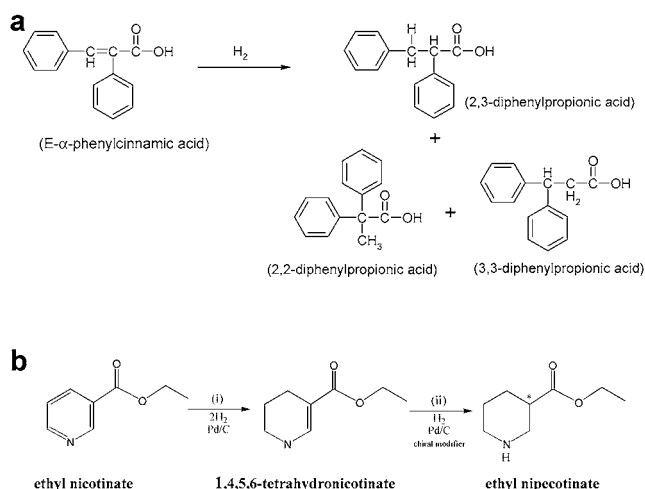
a

b

FIGURE 11. (a) Schematic drawing illustrating the different products arising from the hydrogenation of *E*-α-phenylcinnamic acid. (b) The two-step hydrogenation of ethyl nicotinate to ethyl nipecotinate via 1,4,5,6-tetrahydronicotinate.

Table 2. Enantioselective Hydrogenation of
E-α-Phenylcinnamic Acid (Sequential Approach;
See Text and Figure 6b)[a]

dppf-ferrocenyl-diamine-Pd catalyst	t (h)	conv (%)	TON	product distribution		ee (%)
				A	B	
homogeneous	48	11.5	69	32.5	67.3	35.0
	72	17.2	90	26.0	73.7	24.7
tethered to nonporous silica	48	16.2	215	20.5	79.4	
	72	19.5	238	13.0	86.7	
confined within mesoporous silica (30 Å diameter)	48	35.2	416	31.0	68.8	51.2
	72	39.7	447	26.9	73.0	46.3

[a] Reaction conditions: substrate, 5 g; catalyst, 250 mg; H$_2$ pressure, 20 bar; solvent, methanol/THF = 1:9; temp, 40 °C. Products: A, 2,3- diphenylpropionic acid; B, 2,2-/3,3-diphenylpropionic acid (see Figure 11a).

mesopores of the silica. The exterior surface is first deactivated (as described earlier; see Figure 6), and the inner walls of the pores are derivatized so as to facilitate the subsequent act of tethering (Figure 10). The purpose in tethering a chirally based homogeneous catalyst inside a mesopores is to capitalize on the spatial restrictions imposed upon the reactant by the pore walls so as to boost the enantioselectivity of the reaction to be catalyzed.[3,21]

Proof that such enantioselective enhancement may be generated in this way has been recently demonstrated in the allylic amination of cinnamyl acetate using a chiral catalyst from the ligand 1,1′-bis(diphenylphosphino)-ferrocene (dppf) tethered to the inner walls of mesoporous silica.[3]

Insofar as enantioselective hydrogenations are concerned, we first demonstrated the viability of this kind of constrained, chiral catalyst in the hydrogenation of *E*-α-phenylcinnamic acid (Figure 11a). Next, we attacked the enantioselective catalytic hydrogenation of ethyl nicotinate to ethyl nipecotiniate in a single step, so as to replace the current practice (Figure 11b) that uses a two-step process. Using a Pd(I) dppf-based tethered catalyst, a one-step conversion with an enantioselectivity higher than previously reported was achieved (Tables 2 and 3). And

Table 3. Enantioselective Hydrogenation of
E-α-Phenylcinnamic Acid (Convergent Approach;
See Text and Figure 6b)[a]

dppf-ferrocenyl-diamine-Pd catalyst	t (h)	conv (%)	TON	product distribution		ee (%)
				A	B	
homogeneous	48	23.6	379	83.5	16.8	
	72	38.3	513	76.2	23.1	
tethered to nonporous silica	48	19.8	253	44.1	55.3	36.1
	72	26.0	320	38.4	62.0	27.2
confined within mesoporous silica (30 Å diameter)	48	62.0	526	100		90.7
	72	90.5	715	100		96.5

[a] Reaction conditions: substrate, 5 g; catalyst, 250 mg; H$_2$ pressure, 20 bar; solvent, methanol/THF = 1:9; temp, 40 °C. Products: A, 2,3-diphenylpropionic acid; B, 2,2-/3,3-diphenylpropionic acid (see Figure 11a).

with another constrained, chiral catalyst, this time involving Rh(I), an even better enantioselectivity was achieved.[23]

Scope clearly exists here to improve further the performance of these novel, enantioselective heterogeneous catalysts (for hydrogenations and other reactions). Their prime advantage (over homogeneous analogues) is that they greatly facilitate separation of product from reactant, and are also readily amenable to recycling.

In this Account we have concentrated exclusively on nanoporous silica as the support for anchoring high-performance nanoparticle catalysts. But the general principle may be extended to other solids that have recently been prepared where there are sharply defined nanopores in the range 3−30 nm. Indeed, Joo et al.[24] have recently prepared ordered nanoporous arrays of carbon that support high dispersions of platinum nanoparticles (diameter less than 3 nm) that display promising electrocatalytic activity for oxygen reduction. These nanocatalysts are likely to prove important for fuel cell technologies, based on the proven behavior of other (e.g., Pd−Pt and Pt−Co−Cr)[25] similar systems.

References

(1) Hermans, S.; Raja, R.; Thomas, J. M.; Johnson, B. F. G.; Sankar, G.; Gleeson, D. Solvent-free, low-temperature, selective hydrogenation of polyenes using a bimetallic nanoparticle Ru−Sn catalyst. *Angew. Chem., Int. Ed.* **2001**, *40*, 1211−1215.

(2) Raja, R.; Khimyak, T.; Thomas, J. M.; Hermans, S.; Johnson, B. F. G. Single-step, highly active and highly selective nanoparticle catalysts for the hydrogenation of key organic compounds. *Angew. Chem., Int. Ed.* **2001**, *40*, 4638−4642.

(3) (a) Thomas, J. M.; Maschmeyer, T.; Johnson, B. F. G.; Shephard, D. S. Constrained chiral catalysts. *J. Mol. Catal. A* **1999**, *141*, 139−144. (b) Johnson, B. F. G.; Raynor, S. A.; Shephard, D. S.; Maschmeyer, T.; Thomas, J. M.; Sankar, G.; Bromley, S. T.; Oldroyd, R. D.; Gladden, L. G.; Mantle, M. D. Superior performance of a chiral catalyst confined within mesoporous silica. *Chem. Commun.* **1999**, 1167−1168. (c) Thomas, J. M. Design, synthesis and *in situ* characterization of new solid catalysts. *Angew. Chem., Int. Ed.* **1999**, *38*, 3588−3628.

(4) (a) Shephard, D. S.; Maschmeyer, T.; Johnson, B. F. G.; Thomas, J. M.; Sankar, G.; Ozkaya, D.; Zhou, W. Z.; Oldroyd, R. D. Bimetallic nanoparticle catalysts anchored inside mesoporous silica. *Angew. Chem., Int. Ed. Engl.* **1997**, *36*, 2242−2245. (b) Shephard, D. S.;

Maschmeyer, T.; Sankar, G.; Thomas, J. M.; Ozkaya, D.; Johnson, B. F. G.; Raja, R.; Oldroyd, R. D.; Bell, R. G. Preparation, characterization and performance of encapsulated copper—ruthenium bimetallic catalysts derived from molecular cluster carbonyl precursors. *Chem. Eur. J.* **1998**, *4*, 1214−1224. (c) Raja, R.; Sankar, G.; Hermans, S.; Shephard, D. S.; Bromley, S. T.; Thomas, J. M.; Maschmeyer, T.; Johnson, B. F. G. Preparation and characterisation of a highly active bimetallic (Pd−Ru) nanoparticle heterogeneous catalyst. *Chem. Commun.* **1999**, 1571−1572.

(5) McIndoe, J. S.; Dyson, P. G. *Transition metal carbonyl cluster chemistry*; Gordon and Breach Science Publishers: Amsterdam, The Netherlands, 2000.

(6) (a) Thomas, J. M.; Terasaki, O.; Gai, P. L.; Zhou, W. Z.; Gonzalez-Calbet, J. Structural elucidation of microporous and mesoporous catalysts and molecular sieves by high-resolution electron microscopy. *Acc. Chem. Res.* **2001**, *34*, 583−594. (b) Ozkaya, D.; Zhou, W. Z.; Thomas, J. M.; Midgley, P. A.; Keast, V. J.; Hermans, S. High-resolution imaging of nanoparticle bimetallic catalysts supported on mesoporous silica. *Catal. Lett.* **1999**, *60*, 113−120.

(7) (a) Sinfelt, J. H. *Bimetallic Catalysts: Discoveries, concepts and applications* (Exxon monograph); Wiley: New York, 1983. (b) Davis, R. J.; Boudart, M. Structure of supported Pd−Au clusters determined by x-ray absorption spectroscopy. *J. Phys. Chem.* **1994**, *98*, 5471−5477.

(8) (a) Sankar, G.; Thomas, J. M. *In situ* combined X-ray absorption spectroscopic and X-ray diffractometeric studies of solid catalysts. *Top. Catal.* **1999**, *8*, 1−21. (b) Thomas, J. M.; Sankar, G. The role of XAFS in the *in situ* elucidation of active sites in designed solid catalysts. *J. Synchrotron Radiat.* **2001**, *8*, 55−64.

(9) Midgley, P. A.; Weyland, M.; Thomas, J. M.; Johnson, B. F. G. Z-contrast tomography: A technique in 3-dimensional nanostructural analysis based on rutherford scattering. *Chem. Commun.* **2001**, 907−908.

(10) See, for example: Dagani, R. Tempest in a tiny tube—a critique on hydrogen storage. *Chem. Eng. News* **2002**, *80* (Jan 14), 25−28.

(11) (a) Thomas, J. M.; Raja, R.; Sankar, G.; Johnson, B. F. G.; Lewis, D. W. Solvent-free routes to clean technology. *Chem. Eur. J.* **2001**, *7*, 2973−2978. (b) Thomas, J. M.; Raja, R.; Sankar, G.; Bell, R. G.; Lewis, D. W. Benign by design. New catalysts for an environmentally conscious age. *Pure Appl. Chem.* **2001**, *73*, 1087−1101.

(12) Draths, K. M.; Frost, J. W. Environmentally compatible synthesis of adipic acid from D-glucose. *J. Am. Chem. Soc.* **1994**, *116*, 399−400.

(13) Bromley, S. T.; Sankar, G.; Catlow, C. R. A.; Thomas, J. M.; Johnson, B. F. G.; Maschmeyer, T. New insights into the structure of supported bimetallic nanoclusters catalysts prepared from carbonylate precursors. A combined density functional theory and EXAFS study. *Chem. Phys. Lett.* **2001**, *340*, 524−525.

(14) (a) Rideal, E. K. Catalytic hydrogenations with protected hydrosols. *J. Am. Chem. Soc.* **1920**, *42*, 749−756. (b) Turkevich, J.; Stevenson, P. C.; Hillier, J. A study of the nucleation and growth processes in the synthesis of colloidal gold. *Discuss. Faraday Soc.* **1951**, *11*, 55−61. (c) Thomas, J. M.: Colloidal metals: past, present and future. *Pure Appl. Chem.* **1988**, *60*, 1517−1528.

(15) (a) Zhou, W. Z.; Hunter, H. M. A.; Wright, P. A.; Ge, Q. F.; Thomas, J. M. Imaging the pore structure and polytypic intergrowths in

mesoporous silica. *J. Phys. Chem. B* **1998**, *102*, 6933−6936. (b) Zhao, D. Y.; Huo, Q. S.; Feng, J. L.; Chmelka, B. F.; Stucky, G. D. *J. Am. Chem. Soc.* **1998**, *120*, 6024−6036.

(16) Thomas, J. M.; Sankar, G. The role of synchrotron-based studies in the elucidation and design of active sites in titanium-silica epoxidation catalysts. *Acc. Chem. Res.* **2001**, *34*, 571−581.

(17) (a) Fung, A. S.; Kelley, M. J.; Koningsberger, D. C.; Gates, B. C. Gamma-Al$_2$O$_3$-supported Re−Pt cluster catalysts prepared from [Re$_2$Pt(CO)$_{12}$]: Characterization by extended X-ray absorption fine structure spectroscopy and catalysis of methylcyclohexane dehydrogenation. *J. Am. Chem. Soc.* **1997**, *119*, 5877−5887. (b) Gates, B. C. Models of metal catalysts: beyond single crystals. *Top. Catal.* **2001**, *14*, 173−180. (c) Augustine, S. M.; Sachtler, W. M. H. On the mechanism for the platinum-catalyzed reduction of rhenium in PtRe/Gamma-Al$_2$O$_3$. *J. Catal.* **1989**, *116*, 184−194.

(18) (a) Döbert, F.; Gaube, J. Partial hydrogenation of benzene to cyclohexene in a continuously operated slurry reactor. *Catal. Lett.* **1995**, *31*, 431−438. (b) Nagahara, H.; Ono, M.; Konishi, M.; Fukuoka, Y. Partial hydrogenation of benzene to cyclohexene. *Appl. Surf. Sci.* **1997**, *121*, 448−451. (c) Imamura, H.; Kumai, T.; Nishimura, K.; Nuruyu, T.; Sakata, Y. Partial liquid-phase hydrogenation of benzene to cyclohexene on SiO$_2$-immobilized Eu and Yb catalysts. *Catal. Lett.* **2002**, in press. (d) Ishida, H.; Fukuoka, Y.; Mitsui, O.; Kono, M. Liquid-phase hydration of cyclohexene with highly silicious zeolites. *Stud. Surf. Sci. Catal.* **1994**, *83*, 473−480.

(19) Yang, H.; Gao, H. R.; Angelici, R. J. Hydrogenation of arenes under mild conditions using rhodium pyridylphosphine and bipyridyl complexes tethered to a silica-supported palladium heterogeneous catalyst. *Organometallics* **2000**, *19*, 622−629.

(20) (a) Parshall, G. W.; Ittell, S. D. *Homogeneous Catalysts: The Applications and Chemistry of Catalysis by Soluble Transition Metal Complexes*, 2nd ed.; Wiley-Interscience: New York, 1992. (b) Raja, R.; Sankar, G.; Thomas, J. M. Bifunctional molecular sieve catalysts for the benign ammoximation of cyclohexanone: One-step, solvent-free production of oxime and caprolactam with a mixture of air and ammonia. *J. Am. Chem. Soc.* **2001**, *123*, 8153−8154.

(21) (a) Maschmeyer, T. Unpublished presentation at the Annual Progress Meeting of the Davy Faraday Research Laboratories, 17 March 1995. (b) Thomas, J. M. Tales of tortured ecstasy: Probing the secrets of solid catalysts. *Faraday Discuss.* **1995**, *100*, C9−C27.

(22) Raynor, S. A.; Thomas, J. M.; Raja, R.; Johnson, B. F. G.; Bell, R. G.; Mantle, M. D. A one-step, enantioselective reduction of ethyl nicotinate to ethyl nipecotinate using a constrained, chiral, heterogeneous catalyst. *Chem. Commun.* **2000**, 1925−1926.

(23) Jones, M. D.; Raja, R.; Thomas, J. M.; Rouzard, J.; Johnson, B. F. G.; Lewis, D. W.; Harris, K. D. M. Boosting the enantioselectivity of a novel homogeneous organometallic catalyst by anchoring it inside a mesoporous support. Submitted.

(24) Joo, S. H.; Choi, S. J.; Oh, J.; Kwak, J.; Liu, Z.; Terasaki, O.; Ryoo, R. Ordered nanoporous arrays of carbon supporting high dispersions of platinum nanoparticle. *Nature* **2001**, *412*, 169−172.

(25) Stonehart, P. Development of alloy electrocatalysts for phosphoric acid fuel cells (PAFC). *J. Appl. Electrochem.* **1992**, *22*, 995−1001.

AR990017Q